Rational Design and Synthesis of Novel Dimeric Diketoacid-Containing Inhibitors of HIV-1 Integrase: Implication for Binding to Two Metal Ions on the Active Site of Integrase

Ya-Qiu Long,*,† Xiao-Hua Jiang,† Raveendra Dayam,‡ Tino Sanchez,‡ Robert Shoemaker,‖ Shizuko Sei,§ and Nouri Neamati*,‡

State Key Laboratory of Drug Research, Shanghai Institute of Materia Medica, Shanghai Institutes for Biological Sciences, CAS, 555 Zuchongzhi Road, Shanghai 201203, China, Laboratory of Antiviral Drug Mechanisms, SAIC−Frederick, Screening Technologies Branch, DTP, DCTD, National Cancer Institute at Frederick, Frederick, Maryland 21702, and Department of Pharmaceutical Sciences, School of Pharmacy, University of Southern California, Los Angeles, California 90089

Received November 4, 2003

Discovery of diketoacid-containing compounds as HIV-1 integrase (IN) inhibitors played a major role in validating this enzyme as an important target for the development of therapeutics against HIV infection. In fact, S-1360, the first clinically used IN inhibitor containing a triazole ring as a bioisostere of a carboxylic acid moiety belongs to this class of compounds. To understand the role of divalent metal-chelating in the inhibition of IN (*J. Med. Chem.* **2002**, *45*, 5661−5670), we designed and synthesized a series of novel dimeric diketo-containing compounds with the notion that such dimeric compounds may simultaneously bind to two divalent metal ions on the active site of IN. We rationalized that the two diketo subunits separated by uniquely designed linkers can potentially chelate two metal ions that are either provided from one IN active site or two active sites juxtaposed together in a higher order tetramer. Herein, we show that all the new compounds are highly potent against purified IN with varied selectivity for strand transfer, and that some of the analogues exert potent inhibition of the cytopathic effect of HIV-1 in infected CEM cells. This study represents the first attempt to rationally target two divalent metal ions on the active site of IN and may have potential implications for the design of second generation diketoacid-containing class of inhibitors.

Introduction

Integration of viral cDNA into the host genome is a vital step in the HIV replication cycle. This process is carried out in two distinct enzymatic reactions by HIV-1 integrase (IN).[1,2] In the first step while in the cytoplasm of an infected cell, IN selectively cleaves the terminal dinucleotides (...CA▼GT) from the 3′-ends of the viral DNA in a reaction known as 3′-processing. In the second step, IN transfers viral DNA into host genome wherein terminal 3′-OH of the viral DNA attacks as a nucleophile on the host DNA. This latter step, referred to as strand transfer or integration occurs in the nucleus of the infected cell. Currently, several FDA approved HIV-1 reverse transcriptase and protease inhibitors are available for the treatment of symptomatic HIV disease and acquired immune deficiency syndrome (AIDS).[3] Highly active combination antiretroviral therapy has been very effective in bringing down the viral load; however emergence of multidrug resistant viral strains in infected patients can complicate the response to the treatment.[4] Because of its vital role in the viral replication cycle, the addition of an IN inhibitor to existing components of combination regimen is expected to improve the outcome of therapy.

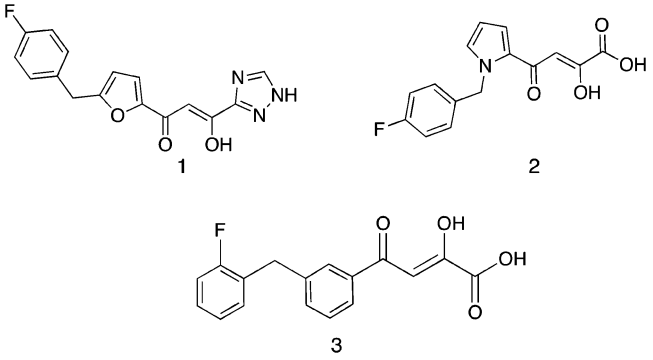

Figure 1. Structures of selected HIV-1 IN inhibitors. Compound **1** (S-1360) is in Phase II clinical trials.

In the past several years, numerous compounds with diverse structural features have been reported as IN inhibitors,[5−7] of which the most developed are a class of compounds with β-diketoacids.[8] Indeed, S-1360 (**1**) was the first drug to enter into clinical trials.[9,10] Several reported β-diketoacids selectively inhibit the strand transfer reaction of IN and exhibit potent antiviral effects against HIV-infected cells. Further studies have indicated that, unlike numerous other IN inhibitors whose antiviral effects can be attributable to non-IN-dependent phenomena,[11,12] members of the β-diketoacid family disrupt viral infectivity in a manner consistent with inhibition of integration.[8] It is believed that the β-diketoacid inhibitors function by competing with substrate DNA in binding to the IN active site.[13] Further structure−activity relationship (SAR) studies were subsequently carried out on β-diketoacids and several novel compounds were found to be active against

* To whom correspondence should be addressed. Y.-Q.L., Phone: 86-21-50806876; fax: +86-21-50807088; e-mail: yqlong@mail.shcnc.ac.cn. N.N., Phone: 323-442-2341; fax: 323-442-1390; e-mail: neamati@usc.edu.

† Shanghai Institute of Materia Medica.

§ Laboratory of Antiviral Drug Mechanisms, SAIC−Frederick, National Cancer Institute.

‖ Screening Technologies Branch, DTP, DCTD, National Cancer Institute.

‡ University of Southern California.

10.1021/jm030559k CCC: $27.50
Published on Web 04/10/2004

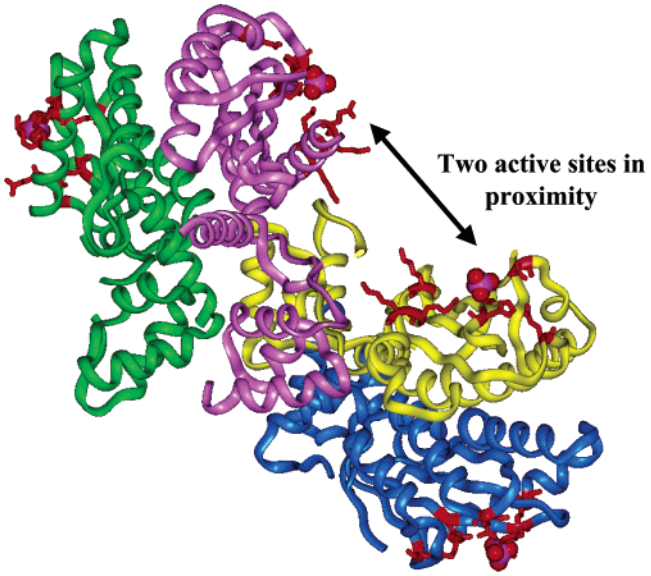

Figure 2. The tetrameric arrangement of IN (core and N-terminal domains; PDB 1K6Y). Each of the colored ribbons represents a monomeric unit of IN. The two adjacent active sites (one from each dimer) are believed to participate together in the integration reactions of IN. The prominent amino acid residues on the IN active site are rendered as red stick models. CPK model shows the phosphate ion near the IN active site.

IN[14−17] (for recent reviews see [5,18]). Compounds **2** and **3** belong to such a new class of β-diketoacid containing compounds collectively referred here as aryl β-diketoacids (ADK).[19]

IN consists of three distinct structural domains: the zinc binding N-terminal, the catalytic core and the DNA binding C-terminal.[20] Structures of each individual domain of IN and the core plus N terminus and core plus C-terminus were previously determined; nevertheless, the X-ray structure of the full-length enzyme has proven to be difficult. The relative spatial arrangement of these structural domains in an intact IN and their interaction with DNA substrates has remained largely unknown. Recently, an X-ray structure of a dimer of IN core domain complexed with an inhibitor was reported, wherein the inhibitor interacted with two crystallograpically related active sites.[21]

Indeed, purified integrases of various retroviruses have been reported to exist as dimers, tetramers, and oligomers in solution.[22−24] It was demonstrated that IN exists in equilibrium between dimeric and tetrameric species in solution.[25] The biochemical and structural studies suggest that a multimer, probably a tetramer of IN, is required for the full integration reaction.[26,27] Two of the four active sites of an active tetramer are involved in the integration reaction, and the other two active site bearing units structurally support the active tetramer. The dimer of dimers observed in the X-ray structure of the IN core and N-terminal domain is a model for a tetrameric unit of IN (Figure 2).[27] In a dimer unit of IN, two active sites are located on the opposite sides of the dimer (Figure 3). These sites never come closer because the monomer−monomer interface is highly hydrophobic in nature and thus energetically

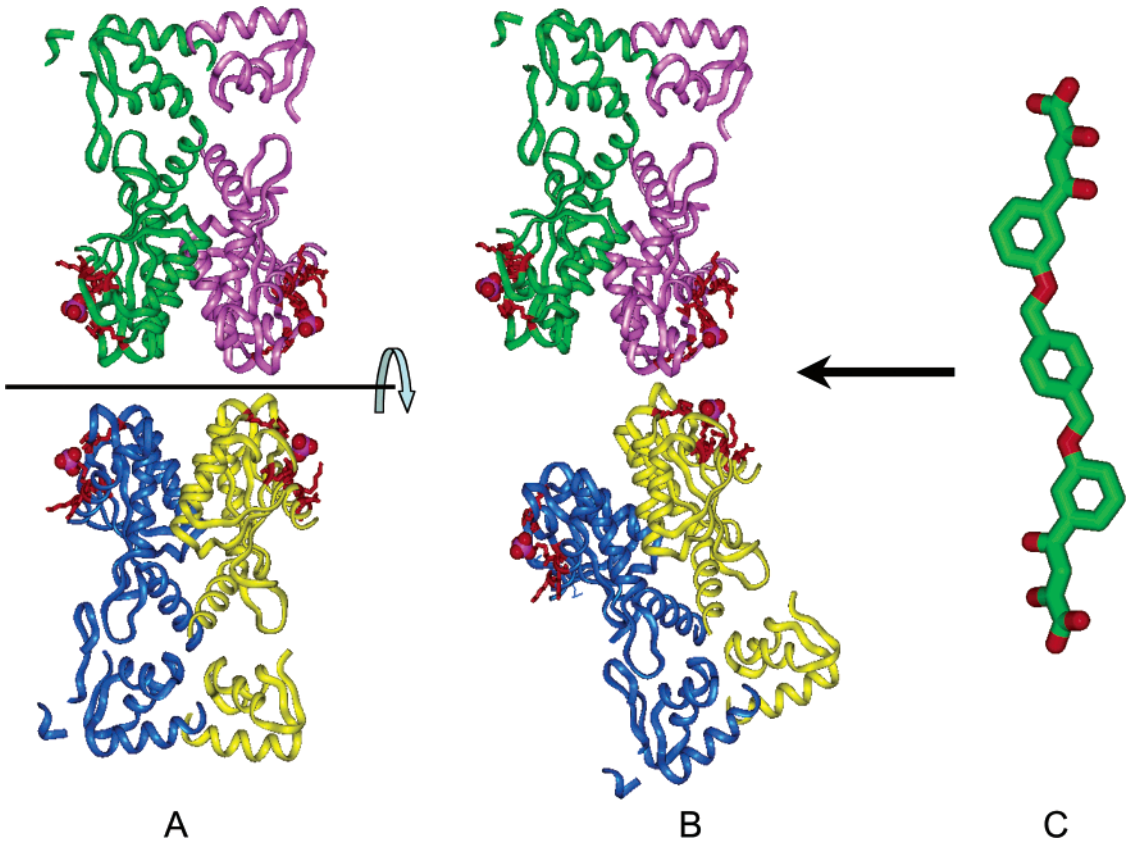

Figure 3. (A) Two dimeric units of IN (N-terminal and core domains; PDB 1K6Y) form a tetrameric complex (B) in such a way that two of the four active sites of tetramer come close and the two adjacent active sites are believed to participate together in the integration reactions of IN. (C) The newly designed benzyloxy-linked ADK dimer (**5c**) is believed to interact with two neighboring active sites of the functional tetramer of IN. The red stick models represent prominent amino acid residues inside the active site of IN while the ribbon models represent N-terminal and core domains of IN. CPK model shows the phosphate ion which is found near the active site of IN (PDB 1K6Y).

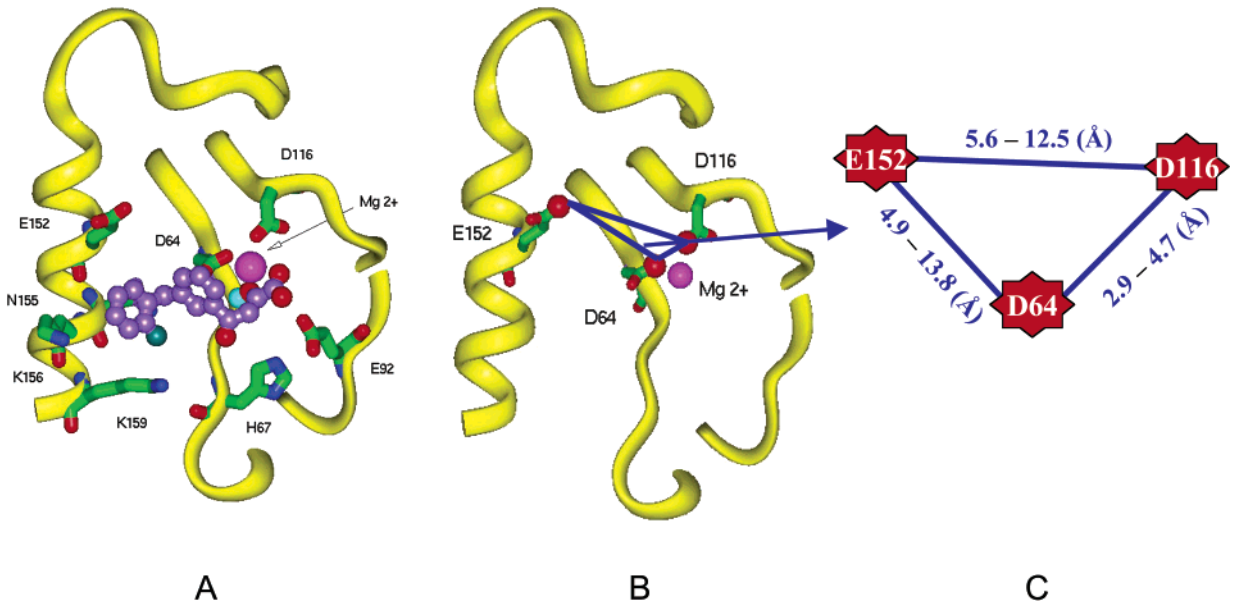

Figure 4. (A) The bound conformation of the compound **3** inside the IN active site. The diketoacid functionality of **3** interacting with Mg^{2+} ion while the aryl part of the compound occupied an area close to E152, N155, K156, and K159. The violet ball-and-stick model represents **3** while the ribbon model shows active site region of the IN. (B) The carboxylate oxygen atoms of the catalytically important amino acid residues E152, D116, and D64 (DD(35)E) are shown as balls on apexes of a triangle (PDB 1BIS). The Mg^{2+} is shown as magenta. (C) The distances between the nearest carboxylate oxygen of E152, D116, and D64 are given in Å.

unfavorable. In the tetramer arrangement, two of the four active sites (one from each dimer) are located close to each other (Figure 2). These active sites are separated by ~40 Å, which is much longer than the five base pair spacing of the sites of insertion of the two viral DNA ends into host DNA. However, the C-terminal domain is missing in this tetramer model, and the relative arrangement of intact IN as a monomer within an active tetramer is unknown. In the functionally relevant tetrameric arrangement of intact IN, these two adjacent active sites probably move close together with the help of certain conformational changes within a dimeric unit of intact IN in order to facilitate integration reactions. Recently, models were proposed for the full-length IN dimer and a tetramer complexed with substrate DNA. The model of the tetrameric arrangement of full-length IN supports the possible involvement of two neighboring active sites from two dimers in integration reactions.[28,29]

Although, the requirement of a metal cofactor for catalysis in IN and many other DNA processing enzymes is well accepted, the number of metal ions and in some cases the type of metal have been the subject of debate for more than three decades.[30] It is generally accepted that Mg^{2+} is a more reasonable cofactor for integration because of its 1 000 000-fold abundance over Mn^{2+} in cells.[30,31] There are also growing and popular notions in support of a two-metal ions theory (for excellent reviews see[32,33]). Even though the X-ray structures show one metal ion on the active site of IN, it is believed that the second metal ion comes with DNA. However, currently there are no IN−DNA complex structures available. After a careful review of the literature we concluded that the second metal ion most likely binds to E152, whereas the first one binds to D64 and D116. The second metal ion can potentially coordinate the carboxylate oxygen atoms of E152 and possibly D64. In a recent molecular dynamics study second Mg^{2+} ion was placed between E152 and D64, and it was found that the second Mg^{2+} was more stable when it was coordinated with an HPO_4^{-2} ion which mimics a portion of the DNA backbone.[34] We further hypothesized that the two metal ions may not have to be present at the active site of IN through its entire enzymatic reaction. For example, the first metal ion, which binds D64 and D116, could play a major role in the 3′-processing reaction, and the second one, which binds to E152, is maybe more relevant during the strand transfer reaction. Sequential metal dependency can also be explained by other situations. Because the smallest subunit required for catalysis is a tetramer of IN, individual monomers could share metal ions. In this scenario, the number of metal ions for a tetrameric complex must be greater than two and less than four.

With an aim to discover novel compounds that could interact with two metal ions[31] within an active site or on adjacently located active sites of a functionally active tetramer of intact IN, we designed two sets of aryl diketoacid dimers (ADK dimers). These dimers displayed an interesting and enhanced inhibitory activity against IN. The selectivity of our novel dimers for strand transfer over 3′-processing reaction varied from 1- to 29-fold. In this study, we describe design, synthesis, SAR, and active site bound conformations of two different sets of ADK dimers.

Design

The rationale behind the design of ADK dimers came mainly from our observations on the bound conformation of compound **3** inside the active site of IN, the relative positions of three catalytically important amino acids residues E152, D116, and D64 at the IN active site, and the tetrameric arrangement of active intact IN. In its bound conformation, the diketoacid moiety of **3** occupied an area near amino acid residues D64, C65 and Mg^{2+}. Subsequently, two of the four oxygen atoms of the diketoacid moiety formed coordination bonds with

Table 1. Distances between the Nearest Carboxylate Oxygen Atoms of the Amino Acid Residues E152, D116, and D64 from the Known Crystal Structures of IN

		amino acid residues (distance in Å)		
PDB accession codes	ref	E152−D116	E152−D64	D116−D64
1B92 (A)[a]	39	5.62[b]	9.31	4.46
1B9D (A)	39	5.56[b]	9.25	4.47
1BI4 (A)	40	9.62	6.57	3.45
1BIS (B)	38	10.90	8.43	4.29
1BIU (A)	38	9.40	7.68	2.93
1BIZ (A)	38	7.40	10.26	4.13
1BL3 (C)	40	7.71	5.00	3.06
1EX4 (A)	37	5.91	4.91	3.71
1K6Y (A)	27	11.90	8.65	3.77
1QS4 (A)	21	10.48	8.28	2.95
2ITG (A)	35	12.54	13.88	4.15
1EXQ (A)	37	11.64	7.53	4.76

[a] The letter in parentheses indicates the subunit of the crystal structure. [b] Please note that several amino acid residues are missing in the active site region of these structures and D64 adopted very different orientation.

Mg^{2+} (Figure 4a). The aryl part of **3** occupied a cavity near residue E152, N155, K156, and K159. The variation in the distance between the nearest pair of carboxylate oxygen atoms of residues E152, D116, and D64 in the reported X-ray structures indicates the flexible nature of a part of the active site which harbors residue E152 (Table 1 and Figure 4b).[21,27,35−40] The closest distance between carboxylate oxygen atoms of D64 and D116 is 2.95 Å in PDB 1QS4, in which Mg^{2+} is coordinated with the carboxylate oxygen atoms of D64 and D116. The difference in the distances between E152 and D116 (5.6 to 12.5 Å) and E152 and D64 (4.9 to 13.8 Å) indicates a possibility that in the presence of a second metal ion the E152 may move closer to D64, and these two amino acid residues hold the second metal ion wherein D64 acts as a bridge between the two metal ions. We rationalized that the diketo functionality of the *β*-diketoacid class of compounds is responsible for metal binding as well as anti-IN activity in isolated enzyme assays and infected cells. On the basis of the bound conformation of **3** and the probable location of the second metal atom between E152 and D64 inside the IN active site, we considered that the introduction of a second diketo moiety onto **3** would significantly affect its activity. Thus, a compound with properly separated diketo moieties could chelate both metal ions at the IN active site. We also hypothesize that the second diketo moiety could interact with the second metal ion on the adjacent active site on the surface of the tetrameric unit. To evaluate these concepts, we designed two sets of ADK dimers, wherein two aryl diketo monomers are connected by various linkers such as cyclic/acyclic diamines and benzyloxy isomers.

Synthesis

Amide-Linked ADK Dimers. The synthesis of the amide-linked ADK dimers was accomplished by coupling the monomer **3** with various diamines. The length and orientation of the linker was designed as described above. Scheme 1 depicts the chemistry employed in the preparation of this series of ADK dimers (synthesis of the piperazine-linked dimer **4a** is shown here as an example). For the preparation of compounds **4a**−**e**, treatment of the 2-fluorobenzaldehyde with 3-bromo-l-lithiobenzene, followed by exposure of the resulting

Scheme 1[a]

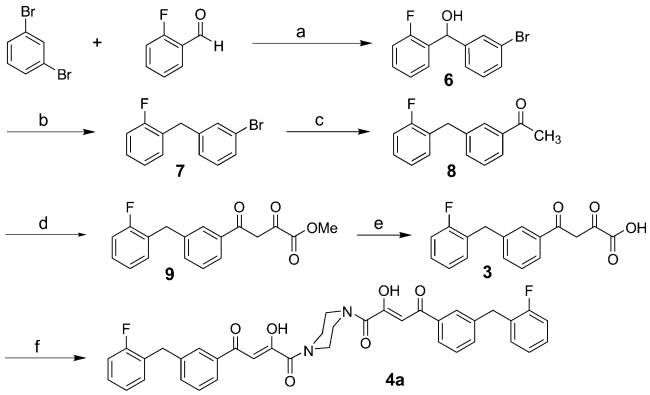

[a] Reagents: (a) *n*-BuLi, THF, −78 °C, 95%; (b) Et_3SiH, BF_3Et_2O, 0 °C, CH_2Cl_2, 0 °C, 84%; (c) *n*-BuLi, DMAc, THF, −78 °C, 63%; (d) CH_3ONa, MeO_2CCO_2Me, toluene/DME = 1:1, 0 °C −60 °C; (e) THF/CH_3OH = 1:1, 1 N NaOH, rt; (d,e two steps overall yield 53.3%) (f) EDCl, HOBt, DMF, 0 °C, piperazine.

Scheme 2[a]

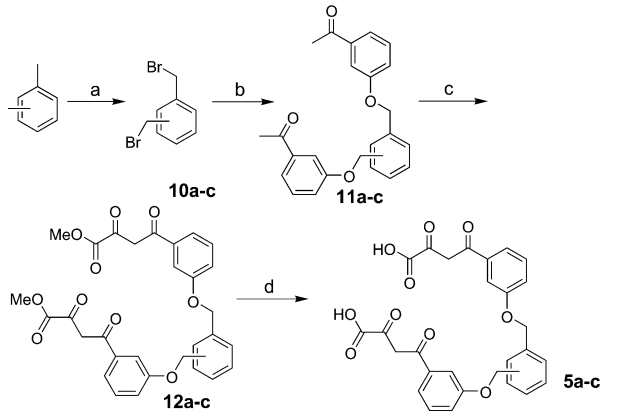

[a] Reagents: (a) Benzoxyl peroxide, NBS, CCl_4; (b) 3-hydroxyacetophenone, K_2CO_3, DMF; (c) MeOOCCOOtBu, CH_3ONa; (d) 1 N NaOH, THF/CH_3OH.

crude adduct **6** to triethylsilane in the presence of boron trifluoride etherate,[41] provided the corresponding 2-fluorobenzylphenyl bromide **7**. Bromide **7** was then lithiated, and the resulting solution was treated with *N*-methoxy-*N*-methylacetamide to provide ketone **8**.[42] Treatment of **8** with dimethyl oxalate and sodium methoxide provided the intermediate ester adduct **9**,[43] which were hydrolyzed in situ to provide the diketo acid **3**. Various diamines were coupled with **3** in the presence of HOBt and EDCI to afford corresponding amide-linked dimers **4a**−**e**.

Benzyloxy-Linked ADK Dimers. The synthesis of benzyloxy-linked ADK dimers **5a**−**d** was achieved in a similar fashion by coupling bis(methyl ketones) **11a**−**c** and **16** with oxalylation agent in the presence of base, with hydrolysis of the resulting bis(methyl esters) **12a**−**c** and **17** being subsequently carried out in the presence of 1 N NaOH in MeOH−THF at room temperature (Scheme 2, 3). Among the methods investigated for oxalylation, *tert*-butyl methyl oxalate in the presence of sodium methoxide proved to be the most effective.[44]

For the synthesis of the benzyloxyl-linked ADK dimers **5a**−**c**, the required bis-acetophenones were prepared by treatment of *m* (*o*, *p*)-xylene with NBS in the presence of benzoxyl peroxide, followed by coupling

Table 2. Inhibition of HIV-1 Integrase Catalytic Activities, Antiviral Activities and GOLD Scores of a Series of Amide-Linked ADK Dimers (**4a**−**e**)

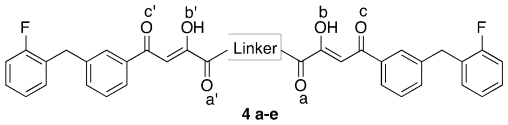

4 a-e

No	Linker	Inhibition of integrase catalytic activities		Antiviral activities [a]							GOLD Score
		3'-processing IC_{50} (μM) [b]	Integration IC_{50} (μM) [b]	SI [c]	EC_{50} (μM) [d]	CC_{50} (μM) [e]	TI [f]	Maximum Protection Dose (μM)	Maximum Protection %	Comments [g]	
4a	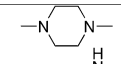	2.5 ± 0.7	0.3 ± 0.2	8	0.8 ± 0.3	11 ± 2	14	2	100	A	73
4b	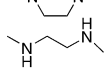	5.8 ± 3.5	0.2 ± 0.1	29	> 5	5	NR [h]	NP [i]		I	76
4c	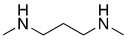	5.3 ± 1.5	0.2 ± 0.1	26	> 9	9	NR	NP		I	73
4d	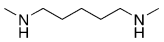	4.8 ± 1.7	0.7 ± 0.4	7	> 12	12	NR	NP		I	77
4e	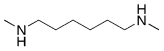	32 ± 9	2.7 ± 2.0	12	16 ± 5	124 ± 1.5	8	20	86	A	71
2		14.5 ± 0.7	0.5 ± 0.1	29							
3		2.5 ± 0.7	0.4 ± 0.3	6	0.02 ± 0.01	62 ± 4	3,111	0.2	98	A	54

[a] Data obtained from the NCI's in vivo anti-HIV primary screen. [b] IC_{50}: Inhibitory concentration 50% (inhibition of purified integrase). [c] SI: Sensitivity index = IC_{50} 3'-processing/IC_{50} integration. [d] EC_{50}: Effective concentration 50% (protection of HIV-1 infected CEM cells). [e] CC_{50}: Cytotoxic concentration 50% (toxicity to uninfected CEM cells). [f] TI: Therapeutic index = CC_{50}/EC_{50}. [g] Comments: NCI designated activity: A (confirmed activity); M (confirmed moderate); I (confirmed inactive). [h] NR: No therapeutic benefit reached due to cytotoxicity. [i] NP: no protection of infected cells.

Scheme 3[a]

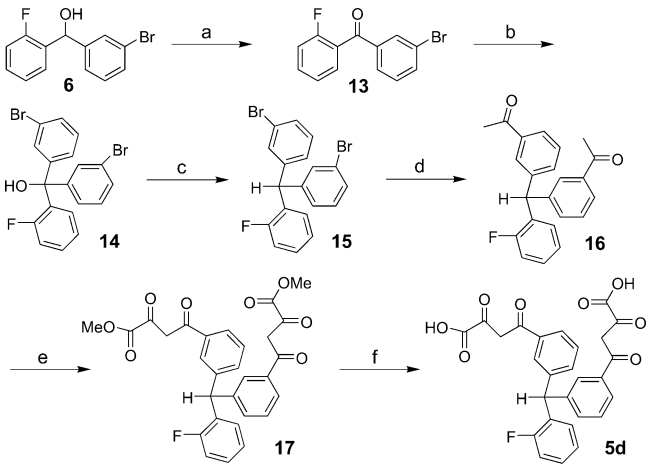

[a] Reagents: (a) Jones reagent; (b) 1,3-dibromobenzene, *n*-BuLi, −78 °C; (c) $(CH_3)_2SiCl_2$, NaI, CH_3CN; (d) *n*-BuLi, THF, −78 °C, *N*-methoxy-*N*-methylacetamide; (e) CH_3ONa, *t*-$BuCO_2CO_2Me$, toluene/DME/THF; (f) 1 N NaOH, THF/CH_3OH.

of the resulting α,α′-dibromo-*m* (*o*, *p*)-xylene **10** with 3-hydroxyacetophenone and potassium carbonate. For the preparation of benzyl-linked dimer **5d**, the required bis-methyl ketone **16** was prepared in four steps (Scheme 3, steps a−d). Oxidation of (3-bromophenyl)(2-fluorophenyl)methanol **6** with Jones reagent provided ketone **13**, which was subsequently coupled with 3-bromol-lithiobenzene. The resulting tertiary alcohol **14** was exposed to dimethylsilane chloride in the presence of sodium iodide and then to a mixture of *N*-methoxy-*N*-methylacetamide and n-BuLi in THF at −78 °C to provide the desired bis-acetophenone **16**.

Results and Discussion

The data from two sets of ADK dimers tested against purified IN and in HIV-1 infected CEM cells are summarized in Tables 2 and 3. All ADK dimers exhibited potent inhibitory activity against IN. The amide-linked dimers (**4a**−**e**) showed a much better selectivity for the strand transfer versus 3′-processing reaction (Figure 5 and Tables 2−3) and a stronger anti-viral efficacy in HIV-infected cells than the benzyloxy-linked ADK dimers (**5a**−**d**).

Inhibitory Activity of Amide-Linked ADK Dimers against IN and HIV-1 Replication. 4-[3-(2-Fluorobenzyl)phenyl]-2-hydroxy-4-oxo-but-2-enoic acid (compound **3**) was selected as the monomer, which formed a series of symmetric dimers with various diamines having different length and orientation. The intrinsic selectivity for strand transfer of these dimeric inhibitors decreased as the length of the linear linker increased from two carbon to six carbon chain (Table 2, compounds **4b**−**e**). Although **4b**−**d** showed high potency and selectivity for strand transfer, they did not show significant antiviral activity. This lack of antiviral activity was due to cytotoxicity for reasons that are not obvious. Compounds **4b**−**d** with CC_{50} values ≤12 μM were among the most toxic analogues. Interestingly, the highly rigid analogue **4a** and the highly flexible **4e** showed somewhat decreased selectivity for strand transfer as compared to **4b** and **4c**. Both compounds exhibit antiviral activity. For example, up to 100% protection of CEM cells from HIV-induced cytopathic effect was achieved with compound **4a** at 2 μM. Although, compound **4e** (EC_{50} = 16 ± 5 μM) was 20-fold less potent than **4a** (EC_{50} = 0.8 ± 0.3 μM) it was 11-fold less toxic than **4a**. In conclusion, the size and shape of the linker had dramatic influence on the strand transfer selectivity, the antiviral activity as well as the toxicity. Further studies are underway in our laboratory to better understand the effect of the linker geometry on activity.

Inhibitory Activity of Benzyloxy-Linked ADK Dimers against IN and HIV-1 Replication in Cell Culture. Two units of 2,4-dioxo-4-phenylbutyric acid were built into the phenyl ring in various substitution patterns, which provided a quick survey of the optimum relative orientation of bis-aryl diketoacid. Among the

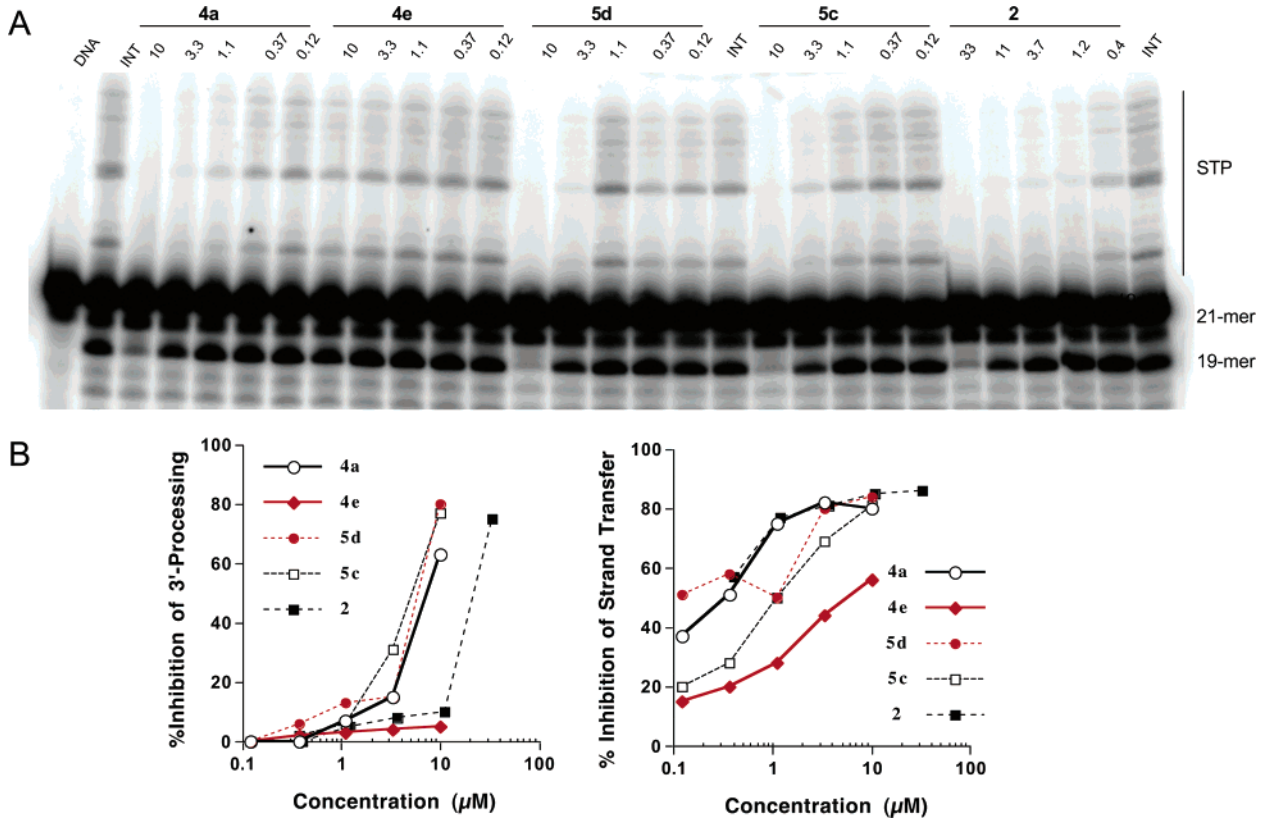

Figure 5. (A) A representative gel showing inhibition of purified IN by selected compounds. A 21-mer blunt-end oligonucleotide corresponding to the U5 end of the HIV-1 LTR, 5′ end-labeled with ^{32}P, is reacted with purified IN. The initial step involves nucleolytic cleavage of two bases from the 3′-end, resulting in a 19-mer oligonucleotide. Subsequently, 3′ ends are covalently joined at several sites to another identical oligonucleotide that serves as the target DNA. This reaction is referred to as strand transfer and the products formed migrate slower than the original substrate (shown in the figure as STP for strand transfer products). Drug concentrations in μM are indicated above each lane. (B) Quantitation of panel A.

Table 3. Inhibition of HIV-1 Integrase Catalytic Activities, Antiviral Activities and GOLD Scores of a Series of Benzyl-Linked ADK Dimers (**5a**−**d**)

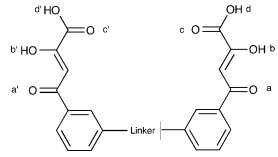

5 a-d

No	Linker	Inhibition of integrase catalytic activities			Antiviral activities [a]						GOLD Score
		3'-processing IC_{50} (μM) [b]	Integration IC_{50} (μM) [b]	SI [c]	EC_{50} (μM) [d]	CC_{50} (μM) [e]	TI [f]	Maximum Protection Dose (μM)	Maximum Protection %	Comments [g]	
5a	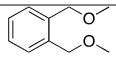	1.8 ± 0.9	0.3 ± 0.2	6	39 ± 3	>200	> 5	63	97	A	69.14
5b	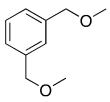	7.3 ± 2.3	0.4 ± 0.1	18	>200	>200	NR [h]	NP [i]		I	66.04
5c	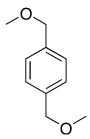	1.7 ± 0.3	1.9 ± 0.1	1	> 200	>200	NR	NP		I	68.92
5d		1.8 ± 0.9	0.2 ± 0.1	9	17 ± 9	81 ± 38	4.8	20	88	A	62.55

[a] Data obtained from the NCI's in vivo anti-HIV primary screen. [b] IC_{50}: Inhibitory concentration 50% (inhibition of purified integrase). [c] SI: Sensitivity index = IC_{50} 3'-processing/IC_{50} integration. [d] EC_{50}: Effective concentration 50% (protection of HIV-1 infected CEM cells). [e] CC_{50}: Cytotoxic concentration 50% (toxicity to uninfected CEM cells). [f] TI: Therapeutic index = CC_{50}/EC_{50}. [g] Comments: NCI designated activity: A (confirmed activity); M (confirmed moderate); I (confirmed inactive). [h] NR: No therapeutic benefit reached due to cytotoxicity. [i] NP: no protection of infected cells.

benzyl-linked bis-phenyl diketoacids (Table 3, compounds **5a**−**c**), the optimum relative orientation of the phenyl diketoacid units is in ortho position. The ortho-substituted bis-phenyl diketoacid **5a** exhibited the most

potent antiviral activity. An interesting feature among these three compounds is their lack of toxicity. Thus, the lack of antiviral activity could be due to two possible explanations. First, these compounds are not stable in cell culture (6 days at 37 °C). Second, the compounds are stable but are not cell permeable. We favor the second explanation because under similar conditions they retain their anti-IN activity. It is interesting to note that compounds **5a** and **5d** showed moderate selectivity against strand transfer but showed potent antiviral activity in HIV-1 infected CEM cells (Figure 5). On the other hand, compound **5b** showed good selectivity for strand transfer but was inactive as an antiviral agent. Compound **5c** with no selectivity for strand transfer was also inactive in cell-based assays (Figure 5). In conclusion, we did not observe a correlation between strand transfer selectivity and antiviral activity. Our future structure−activity relationship studies will shed more light on the nature of strand transfer selectivity and antiviral activity.

Docking Studies. To predict bioactively bound conformation of both sets of ADK dimers, we docked all the compounds into IN active site using GOLD. Currently, there is no structure available for active tetrameric arrangement of intact IN; therefore, we used an active site from a monomeric subunit of IN for docking purposes. The active molecules bound well into IN active site, and formed favorable H-bonding and steric interactions with various active site amino acid residues inside the active site of IN (Tables 2 and 3). The bound conformation of the monomer **3** (with one diketoacid functionality) inside the active site of IN is shown in Figure 4a. The diketoacid moiety of **3** interacts with amino acid residues D64, C65 and with the Mg^{2+} ion while the aryl part of the compound occupied an area close to E152, N155, K156, and K159. An H-bonding interaction is observed between fluoro group of **3** and ϵ-amine of K159. The binding location of **3** is very similar with the bound location of 5CITEP in IN-5CITEP complex crystal structure, but overall positioning of the various functional groups is very different. The diketo moiety of 5CITEP is positioned between E152 and D64, D116 while the diketoacid moiety of **3** interacts with D64, C65 and Mg^{2+} ion. Recent modeling studies revealed that a part (residues 138−149) of IN active site is highly flexible, and remarkable differences are observed in the predicted binding conformation of 5CITEP when compared to bound conformation of 5CITEP in the IN−5CITEP complex crystal structure, as the bound orientation of 5CITEP in crystal structure is influenced by crystal packing effects.[45,46]

Bound Conformation of Amide-Linked ADK Dimers. All the amide-linked ADK dimers bound to almost similar locations inside the IN active site. One of the two diketo moieties (Table 2, superscripted letters a, b, and c) of all the dimers occupied a cavity close to D64, H67, E92, D116, and Mg^{2+}. The oxygen atoms of this diketo group formed coordinate bonds with Mg^{2+} in all the dimers (Table 4). Due to strong metal ligand interactions, this portion of the compound in all the dimers adopted very similar bound conformation. The bound conformations of compounds **4a** and **4d** are shown in Figure 6. The compound **4a** adopted somewhat different bound conformation, as it has a constrained piperazine linker. The carbonyl oxygen atom from the second diketo moiety (Table 2, superscripted letters a′, b′, and c′) formed a strong H-bonding interaction with ϵ-amine of K159 (**4a** C═O···HN K159 (2.27 Å)). This interaction was not observed with the other dimers which possessed a flexible acyclic linker of varying length. Due to difference in the flexibility and size of the linker, the second diketo moiety and its associated aryl part of the dimers adopted quite different bound conformation. The second diketo moiety and its associated aryl part of **4a** occupied an area surrounded by amino acid residues K159, K156, N155, E152, I151, Q62, and D64. In compound **4d**, the second diketo moiety and its associated aryl part of the compound occupied the same area as **4a** and further extended into a space near amino acid residues Q148, P142, I141, and H114.

Table 4. H-Bonding and Mg^{2+}−Ligand Interactions Observed with ADK Dimers

compd	H-bonding interactions (Å)*	Mg^{2+}−ligand interactions (Å)
4a	[a]C═O···HO D116 (2.07)	
	[b]HO···OH C65 (1.96)	[a]C═O···Mg^{2+} (3.01)
	[a′]C═O···HN K159 (2.27)	[b]HO···Mg^{2+} (1.93)
	[c′]C═O···HO D64 (2.44)	[c]C═O···Mg^{2+} (2.12)
4b		[a]C═O···Mg^{2+} (1.91)
	[c′]C═O···HN N62 (2.28)	[b]HO···Mg^{2+} (2.09)
4c		[a]C═O···Mg^{2+} (2.50)
	[b′]HO···HN K159 (2.08)	[b]HO···Mg^{2+} (1.95)
4d		[a]C═O···Mg^{2+} (2.06)
		[b]HO···Mg^{2+} (2.72)
		[c]C═O···Mg^{2+} (1.90)
4e	[a]C═O···HO D64 (2.28)	[a′]C═O···Mg^{2+} (2.04)
	[b′]HO···HN K159 (1.71)	[b]HO···Mg^{2+} (2.02)
5a	-Ph-O′···HN Q62 (2.86)	[b]HO···Mg^{2+} (2.37)
	[b′]OH···O═C D64 (2.05)	[c]C═O···Mg^{2+} (1.77)
	[b′]HO···HN N155 (2.42)	
	[c′]O···HN N155 (2.19)	
	[d′]O···HN K159 (2.04)	
5b	[b′]HO···HN Q62 (1.95)	
	[c′]O···HN Q62 (2.30)	[b]HO···Mg^{2+} (1.65)
	[b′]HO···O═C D64 (2.04)	[d]O···Mg^{2+} (1.91)
	Ph-O···HN K159 (1.67)	
5c		[b]HO···Mg^{2+} (2.22)
	[b]OH···O═C D64 (2.74)	[d]O···Mg^{2+} (1.66)
		[d′]O···Mg^{2+} (2.41)
5d	[c′]O···HN N155 (2.06)	[b]HO···Mg^{2+} (2.31)
	[d′]O···HN K159 (2.08)	[a]O···Mg^{2+} (1.44)
3[b]	[b]OH···O═C C64 (1.41)	[b]HO···Mg^{2+} (1.76)
	F···HN K159 (2.80)	[d]O···Mg^{2+} (2.31)

[a] See Tables 2 and 3 for structures of **4a**−**5d**. Superscripted letters indicate the position of H-bond donor or acceptor atoms. [b] See Figure 1 for compound **3**.

Bound Conformations of Benzyloxy-Linked ADK Dimers. A part of the compound (the diketoacid moiety whose oxygen atoms are denoted by a, b, c, and d (see Table 3)) in all the dimers adopted a quite similar bound conformation and occupied almost same location inside the active site of IN. This part of the compound occupied a space near amino acid residues D64, D116 and Mg^{2+} ion. The oxygen atoms of the diketoacid moiety coordinate with Mg^{2+} ion. The bound conformations of **5a** and **5c** inside the active site of IN are shown in Figure 7. Due to the difference in the linker (benzyloxy isomers), the bound orientation of the second diketoacid moiety (Table 3, a′, b′, c′, and d′) of these dimers is different. The second diketoacid moiety and central benzyloxy group of **5a** occupied a wide cavity surrounded by amino acid residues P142, I151, E152, N155, K159, D64, Q62 and formed several H-bonding interactions with N155, K159, and D64 (Table 4). In case of compound **5b**, the

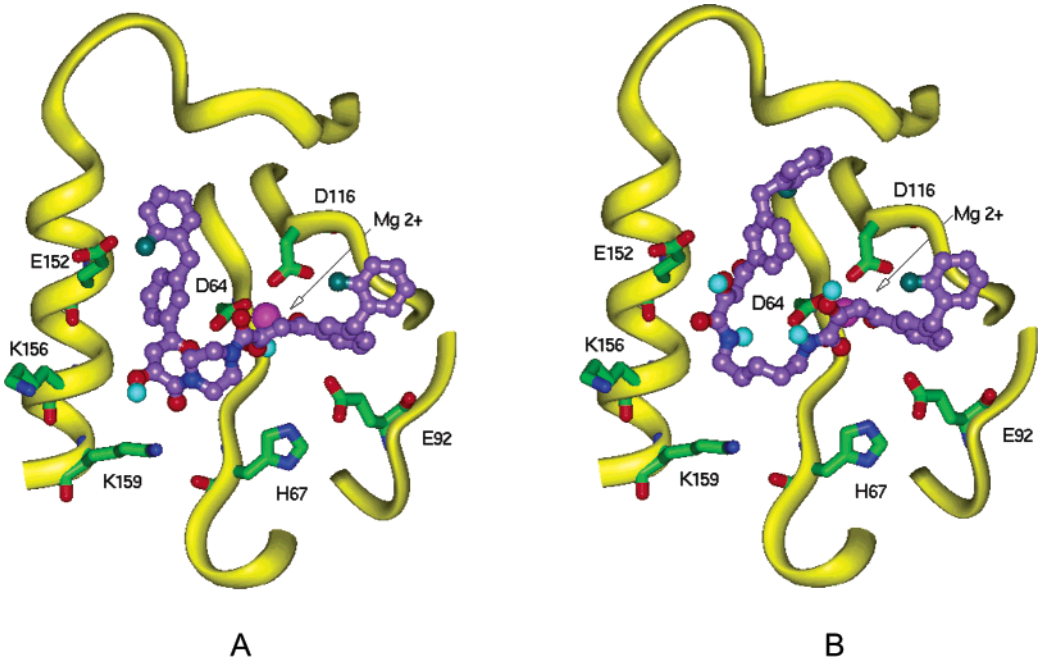

Figure 6. The bound conformations of amide-linked ADK dimers (A) **4a** and (B) **4d** inside the active site of IN. The violet ball-and-stick models represent **4a** and **4d** while the ribbon model represents active site region of the IN. The prominent amino acid residues are rendered as stick models. The Mg^{2+} ion is shown as magenta.

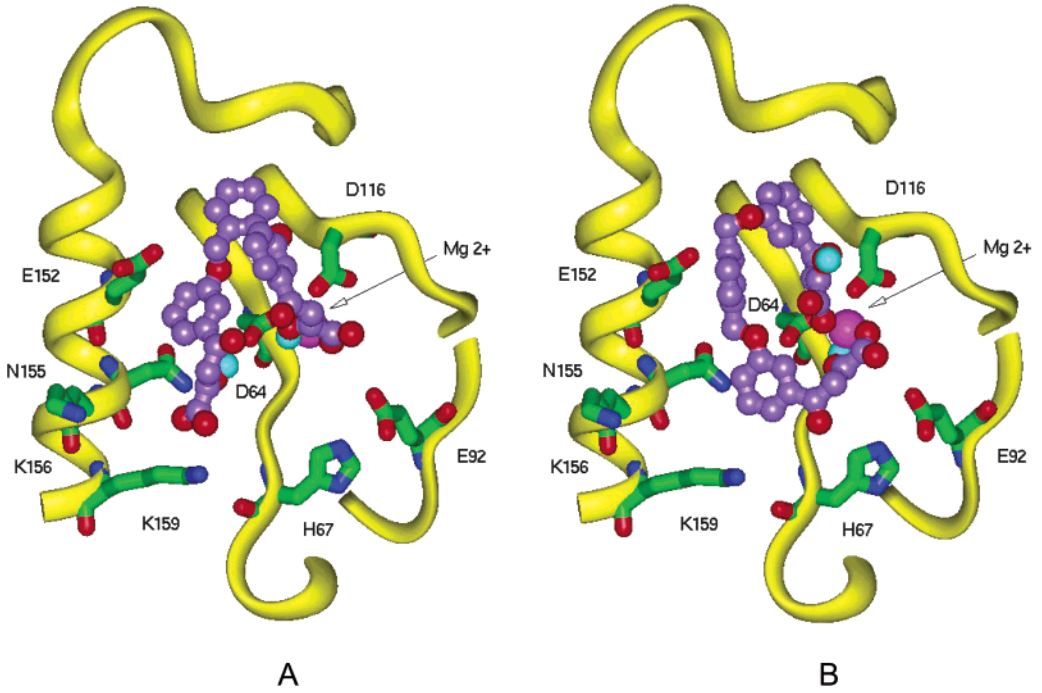

Figure 7. The bound conformations of benzyloxy-linked ADK dimers (A) **5a** and (B) **5c** inside the active site of IN. The violet ball-and-stick models represent **5a** and **5c** while the ribbon model represents the active site region of IN. The prominent amino acid residues at IN active site are rendered as stick models. The Mg^{2+} ion is shown as magenta.

second diketoacid moiety and central benzyloxy group occupied a cavity surrounded by N155, E152, I151, D64, Q62 and formed H-bonding interactions with D64 and Q62. The central benzyloxy group of **5c** occupied an area near N155, E152, I151, and one of the carboxylate oxygen atoms of the second diketoacid moiety coordinates with Mg^{2+} ion (Figure 7B). An H-bonding interaction is observed between the enol hydroxyl of the second diketoacid moiety and D64 (dimer OH···O═C D64 (2.41 Å)). The second diketoacid moiety of **5d** occupied an area near N155, K159, and the metal ligand and H-bonding interactions are given in Table 4.

In summary, the bound conformation of one of the two diketo groups, which interacts with Mg^{2+} ion, is very similar in both sets of ADK dimers. At least two of the three (amide-linked dimers) or four (benzyloxyl-linked dimers) oxygen atoms of this diketo moiety coordinate with Mg^{2+} ion (Table 4). Except **4a**, the second diketo functionality of the amide-linked dimers occupied a cavity close to E152. In the presence of the second metal

ion, the second diketo moiety of these dimers could interact with the second metal ion, which further provides energetically favorable interactions between this set of dimers and IN active site. We also speculate that the second diketoacid moiety of the benzyloxy-linked dimers could interact with an Mg^{2+} ion located on the adjacent active site of a functionally relevant tetrameric IN as the length (the distance between two terminal carboxylate oxygen atoms) of this set of dimers in their extended conformation spans from 18.25 Å (**5d**) to 27.18 (**5c**), which is close to the length of five base pairs on the target DNA.

Conclusions

We have successfully designed and synthesized a series of novel diketo containing compounds to target two metal ions on the active site of IN. Our initial docking studies indicated that one of the diketo groups of ADK dimers interacts with Mg^{2+} ion, while the second diketo moiety occupies an area near E152. Our study shows that the selectivity for strand transfer is important for antiviral activity but not essential. Moreover, the free carboxylate group is not essential for activity either against purified IN or in cell-based assays. Further studies are in progress to optimize the size and the shape of the linker and will be reported in due course.

Experimental Section

Synthesis. General Synthetic Methods. Unless otherwise stated, the ^{1}H NMR spectra were recorded on a Varian 400-MHz spectrometer. The data are reported in parts per million relative to TMS and referenced to the solvent in which they were run. Elemental analyses were obtained using a Vario EL spectrometer. Melting points (uncorrected) were determined on a Buchi-510 capillary apparatus. IR spectra were recorded on Bio-Rad FTS-185 spectrometers. HRMS (EI) spectra were obtained on a Finnigan MAT 95 mass spectrometer. The MS and HRMS (ESI) spectra were obtained on an APEXIII 7.0 T FTMS mass spectrometer. The solvent was removed by rotary evaporation under reduced pressure, and flash column chromatography was performed on silica gel H (10−40 μm). Anhydrous solvents were obtained by redistillation over sodium wire.

Materials, Chemicals, and Enzymes. All compounds were dissolved in DMSO, and the stock solutions were stored at −20 °C. The γ [^{32}P]-ATP was purchased from either Amersham Biosciences or ICN. The expression systems for the wild-type IN and soluble mutant IN^{F185KC280S} were generous gifts of Dr. Robert Craigie, Laboratory of Molecular Biology, NIDDK, NIH, Bethesda, MD.

Preparation of Oligonucleotide Substrates. The oligonucleotides 21top, 5′-GTGTGGAAAATCTCTAGCAGT-3′ and 21bot, 5′-ACTGCTAGAGATTTTCCACAC-3′ were purchased from Norris Cancer Center Core Facility (University of Southern California) and purified by UV shadowing on polyacrylamide gel. To analyze the extent of 3′-processing and strand transfer using 5′-end-labeled substrates, 21top was 5′-end-labeled using T_4 polynucleotide kinase (Epicenter, Madison, WI) and γ [^{32}P]-ATP (Amersham Biosciences or ICN). The kinase was heat-inactivated, and 21bot was added in 1.5-molar excess. The mixture was heated at 95 °C, allowed to cool slowly to room temperature, and run through a spin 25 mini-column (USA Scientific) to separate annealed double-stranded oligonucleotide from unincorporated material.

Integrase Assays. To determine the extent of 3′-processing and strand transfer, wild-type IN was preincubated at a final concentration of 200 nM with the inhibitor in reaction buffer (50 mM NaCl, 1 mM HEPES, pH 7.5, 50 μM EDTA, 50 μM dithiothreitol, 10% glycerol (w/v), 7.5 mM $MnCl_2$, 0.1 mg/mL bovine serum albumin, 10 mM 2-mercaptoethanol, 10% dimethyl sulfoxide, and 25 mM MOPS, pH 7.2) at 30 °C for 30 min. Then, 20 nM of the 5′-end ^{32}P-labeled linear oligonucleotide substrate was added, and incubation was continued for an additional 1 h. Reactions were quenched by the addition of an equal volume (16 μL) of loading dye (98% deionized formamide, 10 mM EDTA, 0.025% xylene cyanol and 0.025% bromophenol blue). An aliquot (5 μl) was electrophoresed on a denaturing 20% polyacrylamide gel (0.09 M Tris-borate pH 8.3, 2 mM EDTA, 20% acrylamide, 8 M urea).

Gels were dried, exposed in a PhosphorImager cassette, and analyzed using a Typhoon 8610 Variable Mode Imager (Amersham Biosciences) and quantitated using ImageQuant 5.2. Percent inhibition (% *I*) was calculated using the following equation:

$$\% I = 100 \times [1 - (D - C)/(N - C)]$$

where *C*, *N*, and *D* are the fractions of 21-mer substrate converted to 19-mer (3′-processing product) or strand transfer products for DNA alone, DNA plus IN, and IN plus drug, respectively. The IC_{50} values were determined by plotting the logarithm of drug concentration versus percent inhibition to obtain concentration that produced 50% inhibition.

Anti-HIV Assays in Cultured Cells. The anti-HIV activity was evaluated in human T cell line CEM-SS infected with HIV-1 as described by Weislow et al.[47] In brief, cells were plated in 96-well plates at 5×10^3 cells/well and infected with HIV-1_{RF} (MOI = 0.3). Serial dilutions of compounds were then immediately added to the cells in a final volume of 200 μL. In each experiment, AZT and dextran sulfate were included as control compounds for anti-HIV activity. The cells were maintained at 37 °C with 5% CO_2-containing humidified air for 6 days. Cell viability was quantified by absorbance at 450 nm after 4 h incubation with 2,3-bis[2-methoxy-4-nitro-5-sulfophenyl]-5-[(phenylamino)carbonyl]-2*H*-tetrazolium hydroxide (XTT) at 0.2 mg/mL. Antiviral activity was graded based on the degree of anti-HIV protection as active (80−100% protection), moderate (50−79% protection), and inactive (0−49% protection). Toxicity of the compounds was determined simultaneously on the same plate in uninfected CEM-SS cells.

Molecular Modeling. The structures of all the compounds (Tables 1 and 2) were built and minimized using Catalyst (Accelrys, Inc). All compounds were modeled in their enol tautomeric form as this form is considered biologically relevant. Compounds **3**, **5a**−**d** were modeled as carboxylates (dianionic form). The poling algorithm implemented within Catalyst was used to generate conformations for all the compounds.[48] For each compound all feasible unique conformations were generated over a 20 kcal/mol range of energies using the best flexible conformation generation method in Catalyst. The subunit B of the core domain X-ray structure of IN (PDB 1BIS) in which all the active site amino acid residues were resolved was chosen for docking purpose. A Mg^{2+} ion was placed in the active site between carboxylate oxygen atoms of amino acid residues D64 and D116 considering the geometry of the Mg^{2+} ion that was present in the subunit A of the IN in PDB 1BIS and subunit A in IN-5CITEP complex X-ray structure (PDB 1SQ4). All the water molecules present in protein were removed, and hydrogen atoms were added to the protein considering appropriate ionization states for both the acidic and basic amino acid residues. Docking was preformed using version 1.2 of the GOLD: Genetic Optimization for Ligand Docking (Cambridge Crystallographic Data Centre) software package.[49] A 12 Å radius active site was defined considering the carboxylate oxygen atom (OD1) of amino acid residue D64 as the center of the active site. All conformers of the compounds were docked into the active site of the IN. On the basis of the GOLD fitness score, for each molecule, a bound conformation with high fitness score was considered as the best bound conformation. All docking runs were carried out using standard default settings with a population size of 100, a maximum number of 100 000 operations, and a mutation and crossover rate of 95. The fitness function that was

implemented in GOLD consisted basically of H-bonding, complex energy, and ligand internal energy terms.

(3-Bromophenyl)(2-fluorophenyl)methanol (6). To a cold solution (−78 °C) of 1.6 M *n*-BuLi in hexanes (6.5 mL, 10.4 mmol) and 20 mL of anhydrous THF was added 1,3-dibromobenzene (1.2 mL, 10.0 mmol) under N_2. The stirred solution was kept below −70 °C. After the reaction was stirred for 2.5 h at this temperature, 2-fluorobenzaldehyde (1.06 mL, 10.4 mmol) was added slowly to keep the temperature below −50 °C. After 0.5 h being stirred at −78 ∼ −50 °C, the reaction mixture was allowed to room temperature and stirred for 3 h. The reaction mixture was poured into aqueous ammonium chloride under stirring and extracted with ether. The organic layer was washed with saturated aqueous $NaHCO_3$ and brine and dried over Na_2SO_4. After removal of the solvent, the residue was chromatographed (15:1 ratio of petroleum ether: ether) to provide 2.81 g of **6** as yellow oil in yield of 95%. ^{1}H NMR ($CDCl_3$): δ 7.59 (s, 1H); 7.39−7.53 (m, 2H); 7.20−7.27 (m, 2H); 7.10−7.19 (m, 2H); 6.95−7.03 (m, 1H); 6.02 (d, 1H); 2.83 (d, 1H).

(3-Bromophenyl)(2-fluorophenyl)methane (7). To a solution of compound **6** (1.183 g, 4.21 mmol) and triethylsilane (0.81 mL, 5.05 mmol) in dichloromethane (15 mL) was added neat boron trifluoride etherate (0.64 mL, 5.05 mmol) under N_2 at 0 °C. The reaction mixture was stirred at room-temperature overnight and then poured into saturated aqueous $NaHCO_3$ and extracted with ether. The combined organic phases were washed with brine and dried over Na_2SO_4. After evaporation, the residue was purified by column chromatography using petroleum ether to afford compound **7** (0.971 g, yield 84%) as yellow oil. ^{1}H NMR ($CDCl_3$): δ 7.35−7.30 (m, 2H); 7.20−7.00 (m, 6H); 3.95 (s, 2H).

1-[3-(2-Fluorobenzyl)phenyl]ethanone (8). To a solution of compound **7** (0.67 g, 2.53 mmol) in THF (10 mL) was added dropwise 1.6 M *n*-butyllithium in hexanes (1.9 mL, 3.03 mmol) under N_2 at −78 °C. The reaction mixture was stirred for 2 h at this temperature, and then *N*,*N*-dimethylacetamide (0.35 mL, 3.80 mmol) was added slowly so that the temperature remained below −50 °C. After 0.5 h being stirred at this temperature, the reaction mixture was poured into aqueous HCl (1N)/ice under vigorous stirring and extracted with ether. The combined organic phases were washed with brine and dried over Na_2SO_4, and the solvent was removed under vacuum. The residue was purified by chromatography using petroleum ether/ethyl acetate (10:1) as eluent to give compound **8** (0.288 g, 63% yield) as yellow oil. ^{1}H NMR ($CDCl_3$): δ 7.83−7.77 (m, 2H); 7.37−7.19 (m, 2H); 7.19−7.15 (m, 2H); 7.14−7.03 (m, 2H); 4.04 (s, 2H); 2.57 (s, 3H). EI-MS *m*/*z*: 228 (M^+).

4-[3-(2-Fluorobenzyl)phenyl]-2,4-dioxobutyric Acid Methyl Ester (9). To a cold solution (0 °C) of CH_3ONa (2.91 g, 53.95 mmol) in dry toluene were added dimethyl oxalate (3.18 g, 26.97 mmol) and compound **8** in dry DME (45 mL) under N_2. The solution was stirred for 0.5 h at 0 °C and then heated to 60 °C overnight. The reaction mixture was quenched with 1.0 N HCl and extracted with EtOAc. The combined organic layers were washed with saturated aqueous $NaHCO_3$ and brine and dried over Na_2SO_4. The solvent was removed under vacuum. The residue was chromatographed using petroleum ether/ethyl acetate (4:1) to give compound **9** as a pale yellow solid. Mp 58−59 °C. ^{1}H NMR ($CDCl_3$): δ 3.94 (s, 3H), 4.07 (s, 3H), 7.05 (s, 1H), 7.03−7.14 (m, 2H), 7.21−7.23 (m, 1H), 7.40−7.47 (m, 2H), 7.82−7.87 (m, 2H). EI-MS *m*/*z*: 314 (M^+). IR (film): 3121, 1726, 1625, 1585, 1266, 1235 cm^{-1}.

4-[3-(2-Fluorobenzyl)phenyl]-2,4-dioxobutyric Acid (3).[19] A solution of compound **9** in THF/CH_3OH (1:1) (40.0 mL) was stirred with 1 N NaOH (40.0 mL, 40.0 mmol) for 1 h at room temperature and then extracted with ether. The water phase was acidified with 2 N HCl to pH 1−2 and extracted with ethyl acetate. The combined organic layers were washed with $NaHCO_3$ and brine and dried over Na_2SO_4, and the solvent was removed under vacuum. The residue was recrystallized from petroleum ether and dichloromethane to give compound **3** as a light yellow solid (1.79 g, two steps overall yield 53.35%). ^{1}H NMR ($CDCl_3$): δ 7.88−7.84 (m, 2H); 7.49−7.42 (m, 2H); 7.25−7.17 (m, 2H); 7.15 (s, 1H); 7.10−7.04 (m, 2H); 4.08 (s, 2H). EI-MS *m*/*z*: 300 (M^+).

4-[3-(2-Fluorobenzyl)phenyl]-1-(4-{4-[3-(2-fluorobenzyl)-phenyl]-2-hydroxy-4-oxobut-2-enoyl}piperazin-1-yl)-2-hydroxy-but-2-ene-1,4-dione (4a). A solution of compound **3** (0.15 g, 0.5 mmol), EDCI (0.101 g, 0.525 mmol), and HOBt (0.071 g, 0.525 mmol) in dry DMF (1.5 mL) was stirred at 0 °C for 15 min. To this solution was added piperazine (0.02 g, 0.23 mmol) in dry DMF. The reaction mixture was stirred for 2.5 h at room temperature and then poured into ice−water and extracted with dichloromethane. The combined organic layers were washed with water and brine and dried over Na_2SO_4. The concentration provided the residue which was purified by chromatography using CH_2Cl_2/CH_3OH (60:1) as eluent to give compound **4a** (0.056 g, 40%) as brown solid. ^{1}H NMR ($CDCl_3$): δ 7.79−7.76 (m, 4H); 7.44−7.38 (m, 4H); 7.25−7.19 (m, 2H); 7.17−7.13 (m, 2H), 7.09−7.03 (m, 4H); 4.05 (s, 4H), 3.73−3.78 (m, 8H). ESI-MS *m*/*z*: 651.1 (M^+ + H, 100); 674.2 (M^+ + Na, 12.0). HR-ESIMS calcd. for $C_{38}H_{32}O_6N_2F_2$+Na: 673.2122, found: 673.2123. Anal. ($C_{38}H_{32}O_6N_2F_2$) C, H, N.

4-[3-(2-Fluorobenzyl)phenyl]-2-hydroxy-4-oxobut-2-enoic Acid (2-{4-[3-(2-fluorobenzyl)phenyl]-2-hydroxy-4-oxobut-2-enoylamino}ethyl)amide (4b). The treatment of aryl diketoacid **3** with ethane-1,2-diamine as described above for the preparation of **4a** provided the desired product **4b** as a pale yellow solid (1.83 g, 65% yield) after chromatography (CH_2Cl_2:CH_3OH = 60:1). ^{1}H NMR ($CDCl_3$): δ 7.87−7.83 (m, 6H); 7.75−7.42 (m, 4H); 7.19 (s, 2H); 7.26−7.02 (m, 6H), 4.05 (s, 4H); 3.64 (m, 4H). ESI-MS *m*/*z*: 625.2 (M^+ + H), 647.2 (M^+ + Na). HR-ESI-MS calcd for $C_{36}H_{30}O_6N_2F_2$ $(M+Na)^+$: 647.1970, found: 647.1975.

4-[3-(2-Fluorobenzyl)phenyl]-2-hydroxy-4-oxobut-2-enoic Acid (3-{4-[3-(2-fluorobenzyl)phenyl]-2-hydroxy-4-oxobut-2-enoylamino}propyl)amide (4c). Compound **4c** was obtained as pale yellow solid in 68% yield according to the same procedure as **4a**. ^{1}H NMR ($CDCl_3$): δ 7.88−7.84 (m, 6H); 7.44−7.38 (m, 4H); 7.21 (s, 1H); 7.24−7.13 (m, 3H), 7.09−7.02 (m, 3H); 4.06 (s, 4H); 3.47 (q, 4H, J = 6.42 Hz); 1.84 (m, 2H). ESI-MS *m*/*z*: 661.4 (M^+ + Na, 100). HR-ESI-MS calcd for $C_{37}H_{32}O_6N_2F_2$ $(M + Na)^+$: 661.2126, found: 661.2105. Anal. ($C_{37}H_{32}O_6N_2F_2$) C, H, N.

4-[3-(2-Fluorobenzyl)phenyl]-2-hydroxy-4-oxobut-2-enoic Acid (5-{4-[3-(2-fluorobenzyl)phenyl]-2-hydroxy-4-oxobut-2-enoylamino}pentyl)amide (4d). Treatment of aryl diketoacid **3** with pentane-1,5-diamine as described above for the preparation of **4a** provided the desired product **4d** as a pale yellow solid (1.2 g, 70% yield) after chromatography (CH_2Cl_2:CH_3OH = 60:1). ^{1}H NMR ($CDCl_3$): δ 7.87−7.82 (m, 4H); 7.44−7.38 (m, 4H); 7.28−7.25 (m, 4H); 7.19 (s, 1H); 7.24−7.13 (m, 3H), 7.09−7.02 (m, 3H); 4.06 (s, 4H); 3.41 (q, 4H, J = 6.86 Hz); 1.69−1.62 (m, 4H); 1.48−1.40 (m, 2H). ESI-MS *m*/*z*: 667.2 (M + H) $^+$, 689.3 (M + Na) $^+$. HR-ESI-MS calcd for $C_{39}H_{36}O_6N_2F_2$ $(M + Na)^+$: 689.2439, found: 689.2445. Anal. ($C_{39}H_{36}O_6N_2F_2$) C, H, N.

4-[3-(2-Fluorobenzyl)phenyl]-2-hydroxy-4-oxobut-2-enoic Acid (6-{4-[3-(2-fluorobenzyl)phenyl]-2-hydroxy-4-oxobut-2-enoylamino}hexyl)amide (4e). Compound **4e** was prepared by coupling aryl diketoacid **3** with hexane-1,6-diamine in a manner similar to **4a.** Purification from chromatography (CH_2Cl_2/CH_3OH = 60:1) afforded a pale yellow solid in yield of 70%. ^{1}H NMR ($CDCl_3$): δ 7.87−7.82 (m, 4H); 7.44−7.38 (m, 4H); 7.19(s, 2H); 7.27−7.13 (m, 5H), 7.09−7.02 (m, 3H); 4.06 (s, 4H); 3.39 (q, 4H, J = 6.73); 1.63−1.60 (m, 4H); 1.43−1.40 (m, 4H). ESI-MS *m*/*z*: 681.3 $(M + H)^+$, 703.4 $(M + Na)^+$. HRMS (ESI) calcd for $C_{40}H_{38}O_6N_2F_2$ $(M + Na)^+$: 703.2596, found: 703.2577. Anal. ($C_{40}H_{38}O_6N_2F_2$) C, H, N.

α,α′-Dibromo-*O*-xylene (10a). Benzoxyl peroxide (18 mg) was added to a solution of NBS (6.675 g, 37.5 mmol) and *O*-xylene (1.85 mL, 15.0 mmol) in CCl_4 (30 mL). The reaction was refluxed for 36 h with stirring. The precipitate was filtered off at room temperature, and the solvent was removed under reduced pressure. The residue was chromatographed with

petroleum ether to give α,α′-dibromo-*o*-xylene as a white solid (1.527 g, yield 33.5%). ^{1}H NMR ($CDCl_3$): δ 7.39−7.36 (m, 2H); 7.33−7.30 (m, 2H); 4.67 (s, 4H).

1-{3-[2-(3-Acetylphenoxymethyl)benzyloxy]phenyl}-ethanone (11a). To the solution of 3-hydroxyacetophenone (0.34 g, 2.5 mmol) in dry DMF (4 mL) were added potassium carbonate (0.71 g, 5.14 mmol) and **10a** (0.264 g, 1.0 mmol) under N_2. The mixture was stirred at 60 °C for 4 h. It was diluted with water and the aqueous mixture extracted with ethyl acetate. The combined organic layers were washed with 2N NaOH and brine and dried over Na_2SO_4. The solvent was removed under reduced pressure. The residue was chromatographed by PE/EtOAC (3:1) to give compound **11a** as a white solid (0.34 g, yield 90.9%). ^{1}H NMR ($CDCl_3$): δ 7.56−7.53 (m, 6H); 7.42−7.34 (m, 4H); 7.17−7.15 (m, 2H), 5.23 (s, 4H); 2.56 (s, 6H). EI-MS (*m*/*z*, %): 374 (M^+).

4-(3-{2-[3-(3-Methoxycarbonyl-3-oxopropionyl)-phenoxymethyl]benzyloxy}phenyl)-2,4-dioxobutyric Acid Methyl Ester (12a). To a solution of CH_3ONa (167 mg, 3.1 mmol) in 1.5 mL of dry toluene were added dropwise compound **11a** (116 mg, 0.31 mmol) and *tert*-butyl methyl oxalate (198 mg, 1.24 mmol) in THF/DME (1.5 mL/1.5 mL) at 0 °C. After being stirred at 0 °C for 0.5 h, the reaction mixture was poured into HCl (1 N)/ice under vigorous stirring and extracted with CH_2Cl_2. The combined organic phases were washed with 1 N HCl brine and dried over Na_2SO_4, and the solvent was removed under vacuum. The residue was purified by chromatography using $CHCl_3/CH_3OH$ (10:1) as eluent to give compound **12a** (0.158 g, yield 93.5%) as yellow solid. Mp 131−134 °C. ^{1}H NMR ($CDCl_3$): δ 3.94 (s, 6H), 5.26 (s, 4H), 7.03 (s, 2H), 7.19 (dt, 2H, J = 8.4, 1.9 Hz), 7.36−7.43 (m, 4H), 7.52−7.56 (m, 4H), 7.58 (s, 2H), 15.19 (br, 1H). ^{13}C NMR (100 MHz, DMSO-d_6): δ 190.09 (×2), 168.47 (×2), 162.02 (×2), 158.68 (×2), 135.78 (×2), 135.02 (×2), 130.31 (×2), 128.98 (×2), 128.18 (×2), 120.82 (×2), 113.45 (×2), 98.36 (×2), 67.67 (×2), 53.07 (×2). IR (film): 3111, 2952, 1734, 1594, 1436, 1283 cm^{-1}.

4-(3-{2-[3-(3-Carboxy-3-oxopropionyl)phenoxymethyl]-benzyloxy}phenyl)-2,4-dioxobutyric Acid (5a). A solution of compound **12a** (0.164 g, 0.30 mmol) in THF/CH_3OH (1:1) (4.0 mL) was treated with 1 N NaOH (3.0 mL, 3.0 mmol). The reaction mixture was stirred for 1 h at room temperature and then extracted with ether. The water phase was acidified with 2 N HCl to pH 1−2 and extracted with ethyl acetate. The combined organic layers were washed with brine and dried over Na_2SO_4, and the solvent was removed under vacuum. The residue was recrystallized from petroleum ether/dichloromethane to give compound **5a** as a pale yellow solid (0.109 g, yield 70.0%). ^{1}H NMR ($CDCl_3$): δ 7.64−7.61 (m, 3H); 7.59−7.55 (m, 3H); 7.49−7.45 (m, 2H); 7.41−7.39 (q, 2H, J = 13.40); 7.35−7.32 (m, 2H); 7.06 (s, 2H), 5.36 (s, 4H). HR-ESI-MS calcd for $C_{28}H_{22}O_{10}$ $(M + Na)^+$: 541.1111; found 541.1113. Anal. ($C_{28}H_{22}O_{10}\cdot 1.7H_2O$) C, H.

α,α′-Dibromo-*m*-xylene (10b). The treatment of *m*-xylene (1.85 mL, 15.0 mmol) with benzoxyl peroxide (23 mg) and NBS (6.675 g, 37.5 mmol) as described above for the preparation of **10a** provided the desired product **10b** as a white solid (1.878 g, yield 47.4%) after chromatography with petroleum ether. ^{1}H NMR ($CDCl_3$): δ 7.40 (s, 1H); 7.31 (m, 3H); 4.46 (s, 4H).

1-{3-[3-(3-Acetyl-phenoxymethyl)benzyloxy]phenyl}-ethanone (11b). Compound **11b** was prepared from the coupling of **10b** (0.396 g, 1.5 mmol) and 3-hydroxyacetophenone (0.51 g, 3.75 mmol) in the presence of potassium carbonate (1.1 g, 7.6 mmol) analogously to compound **11a**. Purification by chromatography (PE/EtOAC = 4:1) produced compound **11b** as a white solid (0.414 g, yield 74.0%). ^{1}H NMR ($CDCl_3$): δ 7.58−7.54 (m, 5H); 7.43−7.36 (m, 5H); 7.20−7.17 (m, 2H); 5.14 (s, 4H); 2.60 (s, 6H). EI-MS (*m*/*z*, %): 374 (M^+).

4-(3-{3-[3-(3-Methoxycarbonyl-3-oxopropionyl)-phenoxymethyl]benzyloxy}phenyl)-2,4-dioxobutyric Acid Methyl Ester (12b). Oxalylation of compound **11b** (238 mg, 0.636 mmol) with MeOOCCOOtBu (407 mg, 2.54 mmol) in the presence of CH_3ONa (343 mg, 6.36 mmol) were performed in a fashion similar to the preparation of **12a** to give compound **12b** (0.343 g, yield 98.7%) as a yellow solid. ^{1}H NMR ($CDCl_3$): δ 3.95 (s, 6H); 5.16 (s, 4H); 7.06 (s, 2H); 7.24−7.21 (m, 2H); 7.45−7.39 (m, 5H); 7.56 (s, 1H); 7.61−7.58 (m, 4H) (an enol proton is not shown in the spectrum). ^{13}C NMR (100 MHz, $CDCl_3$): 190.32 (×2), 168.55 (×2), 162.32 (×2), 158.75 (×2), 136.69 (×2), 136.10 (×2), 129.79 (×2), 128.87 (×2), 127.11 (×2), 126.33 (×2), 120.70, 120.62, 113.26 (×2), 98.23 (×2), 69.97 (×2), 53.26 (×2). Anal. ($C_{30}H_{26}O_{10}$) C, H.

4-(3-{3-[3-(3-Carboxy-3-oxopropionyl)phenoxymethyl]-benzyloxy}phenyl)-2,4-dioxobutyric Acid (5b). Compound **5b** was obtained from the hydrolysis of compound **12b** with 1 N aqueous NaOH solution (3.2 mL, 3.2 mmol) in THF/CH_3-OH (1:1) (4.0 mL) analogously to compound **5a**. Recrystallization from petroleum ether/dichloromethane afforded compound **5b** as a pale yellow solid (0.122 g, yield 73.5%). ^{1}H NMR (DMSO-d_6): δ 7.68−7.63 (m, 4H); 7.51−7.48 (m, 6H); 7.36−7.33 (dd, 2H); 7.09 (s, 2H); 5.23 (s, 4H). HR-ESI-MS calcd for $C_{28}H_{22}O_{10}$ $(M + Na)^+$: 541.111; found: 541.1108. Anal. ($C_{28}H_{22}O_{10}\cdot 1.6H_2O$) C, H.

α,α′-Dibromo-*p*-xylene (10c). Bromination of *p*-xylene (5.56 mL, 112.4 mmol) with NBS (20.1 g, 45.0 mmol) and benzoxyl peroxide (18 mg) provided the desired α,α′-dibromo-*p*-xylene **10c** as a white solid (6.12 g, yield 51.0%) after chromatography (petroleum ether). ^{1}H NMR ($CDCl_3$): δ 7.37 (m, 4H); 4.48 (s, 4H).

1-{3-[4-(3-Acetylphenoxymethyl)benzyloxy]phenyl}-ethanone (11c). Compound **11c** was prepared as a white solid in 36% yield according to the same procedure as **11a**. ^{1}H NMR ($CDCl_3$): δ 7.57−7.54 (m, 4H); 7.47 (s, 4H); 7.39−7.35 (t, 2H); 7.19−7.16 (m, 2H); 5.12 (s, 4H); 2.58 (s, 6H). EI-MS *m*/*z*: 374 (M^+).

4-(3-{4-[3-(3-Methoxycarbonyl-3-oxopropionyl)-phenoxymethyl]benzyloxy}phenyl)-2,4-dioxobutyric Acid Methyl Ester (12c). Compound **12c** was obtained from the oxalylation of compound **11c** in a fashion similar to the preparation of **12a**. Purification from chromatography afforded pure **11c** (0.414 g, yield 100%) as yellow oil. ^{1}H NMR ($CDCl_3$): δ 7.67−7.62 (m, 4H); 7.51−7.47 (m, 6H); 7.36−7.34 (m, 2H); 7.08 (s, 2H); 5.23(s, 4H), 3.85 (s, 6H).

4-(3-{4-[3-(3-Carboxy-3-oxopropionyl)phenoxymethyl]-benzyloxy}phenyl)-2,4-dioxobutyric Acid (5c). Treatment of compound **12c** (0.163 g, 0.298 mmol) with 1 N NaOH as described above for the preparation of **5a** provided the desired product **5c** as a pale yellow solid (0.107 g, yield 69.2%) after recrystallization from petroleum ether and dichloromethane. ^{1}H NMR (DMSO-d_6): δ 7.66−7.61(m, 4H); 7.50−7.46 (m, 5H); 7.34−7.31(m, 3H); 7.08 (s, 2H); 5.21(s, 4H). HR-ESI-MS calcd for $C_{28}H_{22}O_{10}(M + Na)^+$: 541.1111; found: 541.1116. Anal. ($C_{28}H_{22}O_{10}\cdot 1.5H_2O$) C, H.

(3-Bromophenyl)(2-fluorophenyl)methanone (13). To a solution of compound **6** (3.838 g, 13.66 mmol) in acetone 40 mL at 0 °C was added Jones reagent (10.21 mL) dropwise with stirring. The resulting orange solution was stirred under these conditions for 25 min. The cooling bath was then removed, and 2-propanol 10 mL was added dropwise, whereupon a green precipitate formed immediately. The mixture was stirred at room temperature for 10 min and filtered through a short plug of Celite. The flask and the Celite pad were washed with ether. The organic layer was washed with saturated aqueous $NaHCO_3$ and brine and dried over Na_2SO_4. The solvent was removed under vacuum. The residue was purified by chromatography using petroleum ether/ethyl acetate (8:1) as elutent to afford compound **13** (3.757 g, yield 98.6%) as a white solid. ^{1}H NMR (300 MHz, $CDCl_3$): δ 7.98 (s, 1H); 7.97−7.71 (m, 2H); 7.60−7.53 (m, 2H); 7.38−7.29 (m, 2H); 7.21−7.15 (m, 1H). EI-MS *m*/*z*: 278 (M^+). IR (film): 1658, 1608, 1563, 1480, 1453, 1297 cm^{-1}.

Bis(3-bromophenyl)(2-fluorophenyl)methanol (14). To an oven-dried round-bottom flask were added a solution of 1.6 M *n*-BuLi in hexanes (6.5 mL, 10.4 mmol) and 35 mL of dried THF under N_2. The stirred solution was cooled to −78 °C, and to this solution was added 1,3-dibromobenzene (2.28 mL, 18.85 mmol) at such a rate as not allows the temperature to exceed −70 °C. After the reaction was stirred 3.5 h at this temperature, compound **13** in 5 mL of THF was added slowly so that the temperature remained bellowed −50 °C. After being stirred

at −50 °C for 0.5 h, the reaction mixture was allowed to warm slowly to room temperature. Then the reaction mixture was poured into saturated aqueous NH_4Cl under stirring and extracted with ether. The organic layer was washed with saturated aqueous $NaHCO_3$ and brine and dried over Na_2SO_4, and the solvent was removed under vacuum. The residue was purified by chromatography using petroleum ether/ethyl acetate (40:1) as eluent to afford compound **14** (5.58 g, yield 95%) as white glue. ^{1}H NMR (300 MHz, $CDCl_3$): δ 7.67−7.61 (m, 3H); 7.53−6.96 (m, 8H); 6.68−6.67 (m, 1H); 4.41 (s, 1H). EI-MS *m*/*z*: 434 (M^+). IR (film): 1658, 1608, 1563, 1480, 1453, 1297 cm^{-1}.

Bromo-3-((3-bromophenyl)(2-fluorophenyl)methyl)-benzene (15). The compound **14** (5.58 g, 12.79 mmol) and sodium idodide (7.67 g, 51.16 mmol) were stirred in CH_3CN (35 mL) and placed under N_2. To the stirred mixture at room temperature was added dichlorodimethylsilane (3.08 mL, 25.59 mmol) dropwise. The reaction mixture turns dark brown almost immediately, and TLC confirms complete reduction. The mixture was diluted with ethyl acetate and washed with water, saturated aqueous $NaHCO_3$, 10% aqueous sodium thiosulfate, and brine. The solvent was removed under vacuum. The residue was purified by chromatography using petroleum ether as elutent to afford compound **15** (5.37 g, yield 100%) as a white solid. ^{1}H NMR ($CDCl_3$): δ 7.39−7.36 (m, 2H); 7.35−7.13 (m, 5H); 7.12−7.01 (m, 4H); 6.91−6.86 (m, 1H); 5.74 (s, 1H). EI-MS (*m*/*z*, %): 418 (M^+).

1-{3-[(3-Acetylphenyl)(2-fluorophenyl)methyl]phenyl}-ethanone (16). To a solution of compound **15** (1.049 g, 2.497 mmol) in THF (10 mL) was added dropwise of 1.6 M *n*-butyllithium in hexanes (3.9 mL, 6.244 mmol) under N_2 at −78 °C. The reaction mixture was stirred for 45 min at this temperature, and then *N*-methoxy-*N*-methylacetamide (0.70 mL, 6.244 mmol) was added slowly so that the temperature remained below −50 °C. After being stirred for 2 h at this temperature, the reaction mixture was poured into aqueous HCl (1 N)/ice under vigorous stirring and extracted with ether.The combined organic phases were washed with brine and dried over Na_2SO_4, and the solvent was removed under vacuum. The residue was purified by chromatography using petroleum ether/ethyl acetate (10:1) as eluent to give compound **16** (0.522 g, yield 40.2%) as a white solid. ^{1}H NMR (400 MHz, $CDCl_3$): δ 7.86−7.83 (m, 2H); 7.74−7.73 (m, 2H); 7.43−7.40 (t, 2H); 7.30−7.24 (m, 3H); 7.10−7.04 (m, 2H); 6.91−6.87 (td, 1H); 5.94(s, 1H); 2.55 (s, 6H). EI-MS *m*/*z*: 346 (M^+).

4-(3-{(2-Fluorophenyl)[3-(3-methoxycarbonyl-3-oxopropionyl)phenyl]methyl}phenyl)-2,4-dioxobutyric Acid Methyl Ester (17). To an oven-dried round-bottom flask was added CH_3ONa (146 mg, 2.7 mmol) in toluene under N_2. The solution was cooled to 0 °C. To this solution were added MeOOCCOOtBu (173 mg, 4.0 mmol) and compound **16** in dried DME/THF (1:1) (2 mL). The solution was stirred at room temperature for 2 h. The reaction mixture was quenched with 0.1 N HCl and extracted with EtOAc. The combined organic layers were washed with saturated aqueous $NaHCO_3$ and brine and dried over Na_2SO_4, and the solvent was removed under vacuum. The crude product was purified from column chromatography ($CHCl_3$:CH_3OH = 35:1) to give 119 mg of **17** in yield of 85%. Mp 56−58 °C. ^{1}H NMR ($CDCl_3$): δ 7.90−7.88 (d, 2H); 7.78 (s, 2H); 7.49−7.45 (m, 3H); 7.35−7.33 (m, 2H); 7.12−7.06 (m, 2H); 7.01 (s, 1H); 6.91−6.87 (td, 1H); 5.97 (s, 1H); 3.89 (s, 6H). IR (film): 2954, 1736, 1602, 1488, 1436, 1273 cm^{-1}. EI-MS *m*/*z*: 518 (M^+). HRMS calcd for $C_{29}H_{23}FO_8$: 518.1337, found 518.1385.

4-{3-[[3-(3-Carboxy-3-oxopropionyl)phenyl](2-fluorophenyl)methyl]phenyl}-2,4-dioxobutyric Acid (5d). A solution of compound **17** (119 mg) in THF/CH_3OH (1:1) (4.0 mL) was treated with 1 N NaOH (5.0 mL, 5.0 mmol). The reaction mixture was stirred for 1 h at room temperature then extracted with ether. The water phase was acidified with 2 N HCl to pH 1−2 and extracted with ethyl acetate. The combined organic layers were washed with saturated aqueous $NaHCO_3$ and brine and dried over Na_2SO_4, and the solvent was removed under vacuum. The residue was recrystallized from petroleum ether:dichloromethane to give compound **5d** as a pale yellow solid (0.086 g, 76% yield). ^{1}H NMR ($CDCl_3$): δ 7.92−7.80 (m, 4H); 7.49−7.45 (m, 3H); 7.35−7.35 (m, 5H); 7.12−6.91 (m, 3H); 7.00 (s, 1H); 6.09 (s, 1H). ESI-MS *m*/*z*: 489.1 (M^+ − H). Anal. ($C_{27}H_{19}FO_8 \cdot 1.6H_2O$) C, H.

Acknowledgment. We thank Paula Roberts, Quan-En Yang, Omar Ragab, and Carney Chen for their excellent technical assistance. The work in Y.-Q. L.'s laboratory was supported by grants from Shanghai Municipal Committee of Science and Technology, China (02QB14056 and 03DZ19219) and the Chinese Academy of Sciences (KSCX1-SW-11). The work in N.N.'s laboratory was supported by funds from the GlaxoSmithKline Drug Discovery Award. The work in Screening Technologies Blanch was supported by funds from the NCI, under contract number NO1-CO-12400.

Note Added after ASAP Posting. The version of this paper posted April 10, 2004, was missing a double bond in the general structure of Table 3. The keto enol double bond was added to the structure in the corrected version posted April 13, 2004.

References

(1) Brown, P. O. *Integration*; Cold Spring Harbor Press: Cold Spring Harbor, 1999.
(2) Asante-Appiah, E.; Skalka, A. M. HIV-1 integrase: structural organization, conformational changes, and catalysis. *Adv. Virus Res.* **1999**, *52*, 351−369.
(3) De Clercq, E. Strategies in the design of antiviral drugs. *Nat. Rev. Drug Discovery* **2002**, *1*, 13−25.
(4) Richman, D. D. HIV chemotherapy. *Nature* **2001**, *410*, 995−1001.
(5) Neamati, N. Patented small molecule inhibitors of HIV-1 integrase: a ten-year saga. *Expert Opin. Ther. Pat.* **2002**, *12*, 709−724.
(6) Neamati, N. Structure-based HIV-1 integrase inhibitor design: a future perspective. *Expert Opin. Invest. Drugs* **2001**, *10*, 281−296.
(7) Dayam, R.; Neamati, N. Small-Molecule HIV-1 Integrase Inhibitors: the 2001−2002 Update. *Curr. Pharm. Des.* **2003**, *9*, 1789−1802.
(8) Hazuda, D. J.; Felock, P.; Witmer, M.; Wolfe, A.; Stillmock, K.; Grobler, J. A.; Espeseth, A.; Gabryelski, L.; Schleif, W.; Blau, C.; Miller, M. D. Inhibitors of strand transfer that prevent integration and inhibit HIV− 1 replication in cells. *Science* **2000**, *287*, 646−650.
(9) Yoshinaga, T.; Sato, A.; Fujishita, T.; Fujiwara, T. in Vitro Activity of a New HIV-1 Integrase Inhibitor in Clinical Development. *9th Conference on retroviruses and opportunistic infections*: Seattle, 2002.
(10) Billich, A. S-1360 Shionogi-GlaxoSmithKline. *Curr. Opin. Investig. Drugs* **2003**, *4*, 206−209.
(11) Este, J. A.; Cabrera, C.; Schols, D.; Cherepanov, P.; Gutierrez, A.; Witvrouw, M.; Pannecouque, C.; Debyser, Z.; Rando, R. F.; Clotet, B.; Desmyter, J.; De Clercq, E. Human immunodeficiency virus glycoprotein gp120 as the primary target for the antiviral action of AR177 (Zintevir). *Mol. Pharmacol.* **1998**, *53*, 340−345.
(12) Pluymers, W.; Neamati, N.; Pannecouque, C.; Fikkert, V.; Marchand, C.; Burke, T. R., Jr.; Pommier, Y.; Schols, D.; De Clercq, E.; Debyser, Z.; Witvrouw, M. Viral entry as the primary target for the anti-HIV activity of chicoric acid and its tetraacetyl esters. *Mol. Pharmacol.* **2000**, *58*, 641−648.
(13) Espeseth, A. S.; Felock, P.; Wolfe, A.; Witmer, M.; Grobler, J.; Anthony, N.; Egbertson, M.; Melamed, J. Y.; Young, S.; Hamill, T.; Cole, J. L.; Hazuda, D. J. HIV-1 integrase inhibitors that compete with the target DNA substrate define a unique strand transfer conformation for integrase. *Proc. Natl. Acad. Sci. U S A* **2000**, *97*, 11244−11249.
(14) Zhuang, L.; Wai, J. S.; Embrey, M. W.; Fisher, T. E.; Egbertson, M. S.; Payne, L. S.; Guare, J. P., Jr.; Vacca, J. P.; Hazuda, D. J.; Felock, P. J.; Wolfe, A. L.; Stillmock, K. A.; Witmer, M. V.; Moyer, G.; Schleif, W. A.; Gabryelski, L. J.; Leonard, Y. M.; Lynch, J. J., Jr.; Michelson, S. R.; Young, S. D. Design and synthesis of 8-hydroxy-[1,6]naphthyridines as novel inhibitors of HIV-1 integrase in vitro and in infected cells. *J. Med. Chem.* **2003**, *46*, 453−456.

(15) Pais, G. C.; Zhang, X.; Marchand, C.; Neamati, N.; Cowansage, K.; Svarovskaia, E. S.; Pathak, V. K.; Tang, Y.; Nicklaus, M.; Pommier, Y.; Burke, T. R., Jr. Structure Activity of 3-Aryl-1,3-diketo-Containing Compounds as HIV-1 Integrase Inhibitors. *J. Med. Chem.* **2002**, *45*, 3184−3194.
(16) Marchand, C.; Zhang, X.; Pais, G. C.; Cowansage, K.; Neamati, N.; Burke, T. R., Jr.; Pommier, Y. Structural determinants for HIV-1 integrase inhibition by beta-diketo acids. *J. Biol. Chem.* **2002**, *277*, 12596−12603.
(17) Pluymers, W.; Pais, G.; Van Maele, B.; Pannecouque, C.; Fikkert, V.; Burke, T. R., Jr.; De Clercq, E.; Witvrouw, M.; Neamati, N.; Debyser, Z. Inhibition of Human Immunodeficiency Virus Type 1 Integration by Diketo Derivatives. *Antimicrob Agents Chemother.* **2002**, *46*, 3292−3297.
(18) Pais, G. C. G.; Burke, T. R. Novel aryl diketo-containing inhibitors of HIV-1 integrase. *Drugs Future* **2002**, *27*, 1101−1111.
(19) Wai, J. S.; Egbertson, M. S.; Payne, L. S.; Fisher, T. E.; Embrey, M. W.; Tran, L. O.; Melamed, J. Y.; Langford, H. M.; Guare, J. P., Jr.; Zhuang, L.; Grey, V. E.; Vacca, J. P.; Holloway, M. K.; Naylor-Olsen, A. M.; Hazuda, D. J.; Felock, P. J.; Wolfe, A. L.; Stillmock, K. A.; Schleif, W. A.; Gabryelski, L. J.; Young, S. D. 4-Aryl-2,4-dioxobutanoic acid inhibitors of HIV-1 integrase and viral replication in cells. *J. Med. Chem.* **2000**, *43*, 4923−4926.
(20) Esposito, D.; Craigie, R. HIV integrase structure and function. *Adv. Virus Res.* **1999**, *52*, 319−333.
(21) Goldgur, Y.; Craigie, R.; Cohen, G. H.; Fujiwara, T.; Yoshinaga, T.; Fujishita, T.; Sugimoto, H.; Endo, T.; Murai, H.; Davies, D. R. Structure of the HIV-1 integrase catalytic domain complexed with an inhibitor: a platform for antiviral drug design. *Proc. Natl. Acad Sci. U S A* **1999**, *96*, 13040−13043.
(22) Sherman, P. A.; Fyfe, J. A. Human immunodeficiency virus integration protein expressed in *Escherichia coli* possesses selective DNA cleaving activity. *Proc. Natl. Acad. Sci. U S A* **1990**, *87*, 5119−5123.
(23) Jones, K. S.; Coleman, J.; Merkel, G. W.; Laue, T. M.; Skalka, A. M. Retroviral integrase functions as a multimer and can turn over catalytically. *J. Biol. Chem.* **1992**, *267*, 16037−16040.
(24) Vincent, K. A.; Ellison, V.; Chow, S. A.; Brown, P. O. Characterization of human immunodeficiency virus type 1 integrase expressed in *Escherichia coli* and analysis of variants with amino- terminal mutations. *J. Virol.* **1993**, *67*, 425−437.
(25) Jenkins, T. M.; Engelman, A.; Ghirlando, R.; Craigie, R. A soluble active mutant of HIV-1 integrase: involvement of both the core and carboxyl-terminal domains in multimerization. *J. Biol. Chem.* **1996**, *271*, 7712−7718.
(26) Heuer, T. S.; Brown, P. O. Photocross-linking studies suggest a model for the architecture of an active human immunodeficiency virus type 1 integrase-DNA complex. *Biochemistry* **1998**, *37*, 6667−6678.
(27) Wang, J. Y.; Ling, H.; Yang, W.; Craigie, R. Structure of a two-domain fragment of HIV-1 integrase: implications for domain organization in the intact protein. *EMBO J.* **2001**, *20*, 7333−7343.
(28) De Luca, L.; Pedretti, A.; Vistoli, G.; Barreca, M. L.; Villa, L.; Monforte, P.; Chimirri, A. Analysis of the full-length integrase-DNA complex by a modified approach for DNA docking. *Biochem. Biophys. Res. Commun.* **2003**, *310*, 1083−1088.
(29) Podtelezhnikov, A. A.; Gao, K.; Bushman, F. D.; McCammon, J. A. Modeling HIV-1 integrase complexes based on their hydrodynamic properties. *Biopolymers* **2003**, *68*, 110−120.
(30) Cowan, J. A. *The Biological Chemistry of Magnesium*; VCH: 1995; pp 1−23.
(31) Neamati, N.; Lin, Z.; Karki, R. G.; Orr, A.; Cowansage, K.; Strumberg, D.; Pais, G. C.; Voigt, J. H.; Nicklaus, M. C.; Winslow, H. E.; Zhao, H.; Turpin, J. A.; Yi, J.; Skalka, A. M.; Burke, T. R., Jr.; Pommier, Y. Metal-dependent inhibition of HIV-1 integrase. *J. Med. Chem.* **2002**, *45*, 5661−5670.
(32) Steitz, T. A. DNA polymerases: structural diversity and common mechanisms. *J. Biol. Chem.* **1999**, *274*, 17395−17398.
(33) Steitz, T. A. A mechanism for all polymerases. *Nature* **1998**, *391*, 231−232.
(34) Lins, R. D.; Adesokan, A.; Soares, T. A.; Briggs, J. M. Investigations on human immunodeficiency virus type 1 integrase/DNA binding interactions via molecular dynamics and electrostatics calculations. *Pharmacol. Ther.* **2000**, *85*, 123−131.
(35) Bujacz, G.; Alexandratos, J.; Qing, Z. L.; Clement-Mella, C.; Wlodawer, A. The catalytic domain of human immunodeficiency virus integrase: ordered active site in the F185H mutant. *FEBS Lett.* **1996**, *398*, 175−178.
(36) Dyda, F.; Hickman, A. B.; Jenkins, T. M.; Engelman, A.; Craigie, R.; Davies, D. R. Crystal structure of the catalytic domain of HIV-1 integrase: similarity to other polynucleotidyl transferases. *Science* **1994**, *266*, 1981−1986.
(37) Chen, J. C.; Krucinski, J.; Miercke, L. J.; Finer-Moore, J. S.; Tang, A. H.; Leavitt, A. D.; Stroud, R. M. Crystal structure of the HIV-1 integrase catalytic core and C-terminal domains: a model for viral DNA binding. *Proc. Natl. Acad. Sci. U.S.A.* **2000**, *97*, 8233−8238.
(38) Goldgur, Y.; Dyda, F.; Hickman, A. B.; Jenkins, T. M.; Craigie, R.; Davies, D. R. Three new structures of the core domain of HIV-1 integrase: an active site that binds magnesium. *Proc. Natl. Acad. Sci. U.S.A.* **1998**, *95*, 9150−9154.
(39) Greenwald, J.; Le, V.; Butler, S. L.; Bushman, F. D.; Choe, S. The mobility of an HIV-1 integrase active site loop is correlated with catalytic activity. *Biochemistry* **1999**, *38*, 8892−8898.
(40) Maignan, S.; Guilloteau, J. P.; Zhou-Liu, Q.; Clement-Mella, C.; Mikol, V. Crystal structures of the catalytic domain of HIV-1 integrase free and complexed with its metal cofactor: high level of similarity of the active site with other viral integrases. *J. Mol. Biol.* **1998**, *282*, 359−368.
(41) Smonou, I. One step reduction of diaryl ketones to hydrocarbons by etherated boron trifluoride-triethylsilane system. *Synth. Commun.* **1994**, *24*, 1999−2002.
(42) Nahm, S.; Weinreb, S. M. N-Methoxy-*N*-methylamides as effective acylating agents. *Tetrahedron Lett.* **1981**, *22*, 3815−3818.
(43) Bachmann, W. E.; Cole, W.; Wilds, A. L. The total synthesis of the sex hormone Equilenin and its stereoisomers. *J. Am. Chem. Soc.* **1940**, *62*, 824−839.
(44) Jiang, X. H.; Song, L. D.; Long, Y. Q. Highly Efficient Preparation of Aryl beta-Diketo Acids with *tert*-Butyl Methyl Oxalate. *J. Org. Chem.* **2003**, *68*, 7555−7558.
(45) Sotriffer, C. A.; Ni, H.; McCammon, A. J. HIV-1 Integrase inhibitor interactions at the active site: prediction of binding modes unaffected by crystal packing. *J. Am. Chem. Soc* **2000**, *122*, 6136−6137.
(46) Barreca, M. L.; Lee, K. W.; Chimirri, A.; Briggs, J. M. Molecular Dynamics Studies of the Wild-Type and Double Mutant HIV-1 Integrase Complexed with the 5CITEP Inhibitor: Mechanism for Inhibition and Drug Resistance. *Biophys. J.* **2003**, *84*, 1450−1463.
(47) Weislow, O. W.; Kiser, R.; Fine, D.; Bader, J.; Shoemaker, R. H.; Boyd, M. R. New soluble-formazan assay for HIV-1 cytopathic effects: application to high-flux screening of synthetic and natural products for AIDS antiviral activity. *J. Natl. Cancer Inst.* **1989**, *81*, 577−586.
(48) Smellie, A.; Teig, S. L.; Towbin, P. Poling − Promoting Conformational Variation. *J. Comput. Chem.* **1995**, *16*, 171−187.
(49) CCDC, C. C. E., UK *GOLD*; 1.2 ed.

JM030559K